Turkish Journal of Electrical Engineering & Computer Sciences

http://journals.tubitak.gov.tr/elektrik/

Research Article

Turk J Elec Eng & Comp Sci
(2019) 27: 4390 – 4402

doi:10.3906/elk-1904-171

Decoupling network for Tx/Rx body coil for 7T MRI

Ashraf ABUELHAIJA[1,*], **Sana SALAMH**[2], **Osama NASHWAN**[1]
[1]Department of Electrical Engineering, Faculty of Engineering, Applied Science Private University, Amman, Jordan
[2]Department of Telecommunication Engineering, Faculty of Engineering, Arab American University, Jenin, Palestine

Received: 24.04.2019 • **Accepted/Published Online:** 25.07.2019 • **Final Version:** 26.11.2019

Abstract: The parallel imaging technique is widely used in 7T MRI scanners. It employs multichannel RF coil arrays to apply a concurrent excitation and acquisition method. Concurrent excitation faces significant challenges in terms of electromagnetic coupling between the RF coil elements. In order to prevent interference between the RF coil elements' exciters, several decoupling methods have been developed to compensate for coupling and to permit independent work for the exciters. This paper studies the coupling between meander coils arranged in two different geometrical setups and investigates the isolation performance between the coils by applying two different decoupling networks depending on the geometrical setup of the coils. These two decoupling networks in addition to a T-shaped decoupling network have been integrated into a Tx/Rx body coil for 7 T to compensate for mutual coupling between array coil elements. The results have been obtained by using CST Microwave Studio (CST AG, Darmstadt, Germany).

Key words: Magnetic resonance imaging, 7-Tesla, mutual coupling, decoupling network, radiofrequency coils, resonant circuit, transmit/receive coil

1. Introduction

Ultrahigh magnetic field MRI scanners (e.g., 7T) are considered valuable and promising diagnostic tools due to the higher obtainable signal-to-noise ratio (SNR) and image quality [1–3]. In contrast, the exciting frequency required to examine the protons in the human body increases. This increase leads to significant distortion in the field distribution (inhomogeneity) inside human tissues [4, 5]. Several approaches have been proposed to overcome the inhomogeneity of field distribution. The most famous and promising approaches are static RF shimming [6, 7], transmit SENSE [8, 9], and TIAMO [10]. All these approaches use multichannel parallel RF transmission methods. These methods utilize different RF coil array elements such as ceramic resonators [11], loops [12, 13], microstrip lines (MSLs) [14], dipole antennas [15], and monopoles [16].

An optimal implementation of this method requires good isolation between the array elements. In order to reduce and eliminate the mutual coupling, several decoupling methods have been proposed and developed. In an earlier study on phased-array design, conventional decoupling techniques such as coil overlapping were used to minimize the coupling between nearest-neighbor coils, whereas low input impedance preamplifiers were used to decouple the nonnearest neighbors [17]. In [18], a new decoupling method was based on the assumption that any n-element phased array can be decoupled by a 2n-port interface system. Simulation results in [19] showed that a decoupling matrix can be inserted between the power amplifiers and the transmit array to achieve ideal decoupling. Reactive decoupling networks have been developed to be inserted between the adjacent coil

*Correspondence: ashrafabuelhaija@googlemail.com

elements in order to compensate for mutual coupling [20–22]. A parasitic element-based decoupling method has been demonstrated as a successful decoupling technique for microstrip transmission line array elements [23], monopole elements [24], and phased array [25]. Another technique that has played an intrinsic role in transmit array decoupling is an ultralow output impedance RF power amplifier [26]. This amplifier with its unique property has the capability of decoupling the transmit coil elements as well as delivering maximum RF power. Feedback loops have also been developed to reduce the coupling between the transmit coil elements [27].

This paper is organized as follows: the second section presents the advantages of using microstrip transmission line resonators in ultrahigh MRI scanners. Section 3 derives equivalent circuit models for two different arrangements of meander coils: parallel aligned and collinear aligned. Section 4 presents three different decoupling networks designed for three different geometrical setups of the coils. These decoupling networks have been used to decouple a 32-channel body coil for 7 T.

2. Theory

2.1. Microstrip transmission line resonator

Since the demand for using MRI scanners with their property of ultrahigh magnetic field strength has increased, the challenge of designing RF coils started. These scanners increase the frequency of the excitation signal required to excite the nuclei of protons in the human body. Once the frequency increases, the radiation losses will increase as a consequence.

Researchers have been able to overcome this challenge by developing microstrip transmission line resonators. These resonators have demonstrated high Q-factor as well as signal-to-noise ratio (SNR) [28]. In order to improve the penetration characteristics of this resonator, two meanders have been added at both ends of the conductors [29]. For safety, these meanders have been loaded by high-dielectric materials [30].

The geometry of this resonator in free space is shown in Figure 1a. The two conductors of the resonator have been printed on FR-4 substrate ($\varepsilon_r = 4.4$, $\tan\delta = 0.02$) with a thickness of 0.5 mm and dimensions of 250 mm $\times$ 10 0mm. A ground plane is placed 20 mm apart on the opposite side. Dielectric substrates ($\varepsilon_r = 10.2$, $\tan\delta = 0.0023$) of 3.2 mm in thickness have been used to load the meanders. On the upper side, dielectric substrates with dimensions of 80 mm $\times$ 20 mm have been placed, whereas dielectric substrates with dimensions of 7 0mm $\times$ 16 mm have been placed on the backside. A homogeneous phantom ($\varepsilon_r = 45.3$, $\sigma = 0.8$ S/m) with dimensions of 600 mm $\times$ 90 mm $\times$ 370 mm is placed at a distance of 200 mm above the resonator. More details concerning this resonator were presented in [31].

Meander coil parameters such as reflection coefficient, input impedance, and Q-factor have been carried out based on CST Microwave Studio FDTD software. From EM simulation, it was found that our coil can be represented as a series RLC resonant circuit due to its impedance behavior. The resonant frequency of 298 MHz and the Q-factor of 69 obtained by the EM simulation have been used in the design of the equivalent circuit model as initial values, whereas the coil resistance and reactance components are strongly dependent on them, as shown in the following equations:

$$f_o = \frac{1}{2\pi\sqrt{LC}} \tag{1}$$

and

$$Q = \frac{1}{R_d} \cdot \sqrt{\frac{L}{C}}, \tag{2}$$

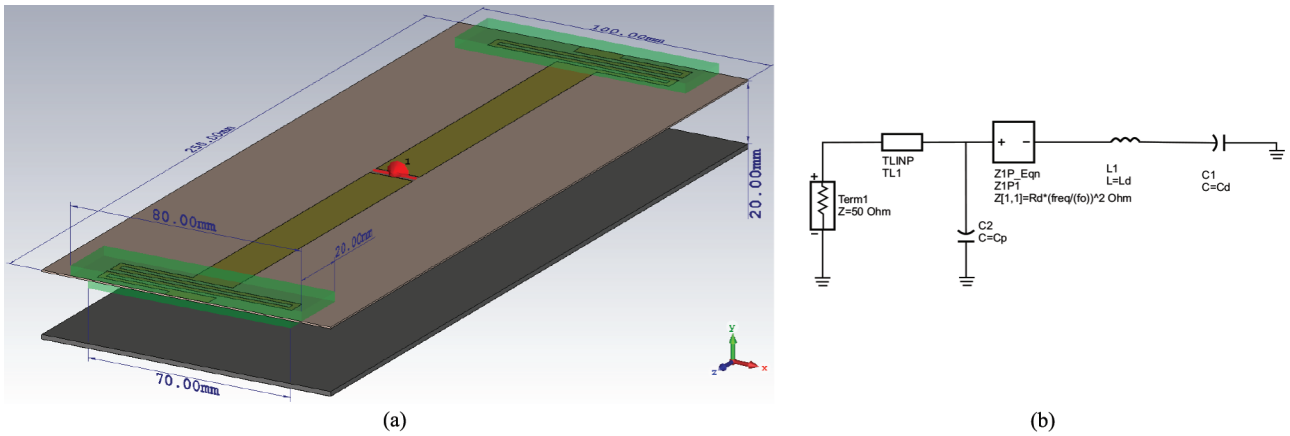

(a) (b)

Figure 1. Single meander coil: (a) geometry of the meander coil, (b) equivalent circuit model of a single meander coil.

where f_o is the resonant frequency, Q is the quality factor, R_d is the coil resistance, L is the self-inductance, and C is the self-capacitance.

Optimization goals in a circuit model including the initial conditions as well as good agreement between EM simulation and circuit simulation using the Advanced Design System (ADS simulator) will lead us to an equivalent circuit model as shown in Figure 1b. The coil resistance R_d of 5.9 ohm has been modeled as frequency-dependent for better results, the coil inductance L_d" is 205.76 nH, and the coil capacitance C_d is 1.3839 pF. Shunt capacitor C_p of 3.36 pF represents the parasitic capacitance of the coil. The quarter wave length coaxial cable (TL1) is used to match the low input impedance of the coil to a 50-ohm generator. Good agreement between results of the meander coil reflection coefficient and input impedance from EM and circuit simulations has been achieved, as shown in Figures 2a and 2b, respectively.

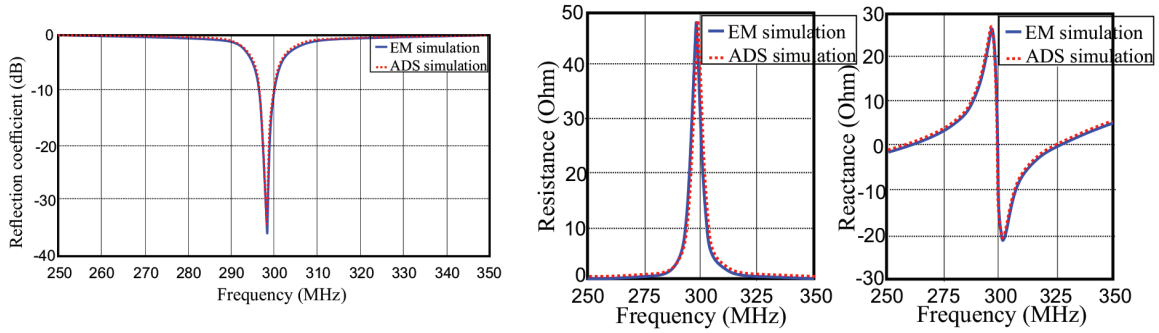

(a) (b)

Figure 2. Single meander coil parameters: (a) reflection coefficient of meander coil, (b) input impedance of single meander coil (left) resistance, (right) reactance.

2.2. Equivalent circuit model of coupled meander coils

2.2.1. Parallel meander coils

In Figure 3, two-coupled meander coils parallel aligned in free space below a homogeneous phantom are shown. Based on the full-wave simulation results, the S and Z parameter matrices for two-element array have been obtained as follows:

$$S = \begin{bmatrix} -0.8104 - j * 0.0004 & 0.1185 - j * 0.0702 \\ 0.1185 - j * 0.0702 & -0.8104 - j * 0.0004 \end{bmatrix}, \tag{3}$$

$$Z = \begin{bmatrix} 5.3879 - j * 0.2929 & 3.6137 - j * 2.1678 \\ 3.6137 - j * 2.1678 & 5.3879 - j * 0.2929 \end{bmatrix}. \quad (4)$$

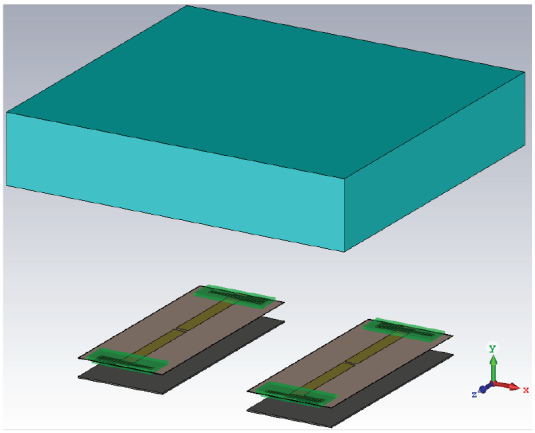

Figure 3. Simulation setup for two parallel meander coils in free space with a gap of 100 mm, situated 200 mm below a homogeneous phantom.

It is clear from the above matrices that our network possesses both symmetrical and reciprocal properties. This will ease our task of building the equivalent network of the coupled elements. The second observation comes from the impedance matrix, where the mutual reactance between both elements is capacitive. Because our meander coil can be equivalently represented as a resonator, as we have already seen in Figure 1b, it is possible to model multiple element coils as coupled resonators. From antenna theory, two common equivalent networks can model the coupling between elements: the tee-network and the pi-network, as shown in Figure 4, where Z_{11} is the self-impedance of element 1, Z_{22} is the self-impedance of element 2, Z_{21} is the mutual impedance between both elements, Z_1 is the input impedance to element 1, and Z_2 is the input impedance to element 2.

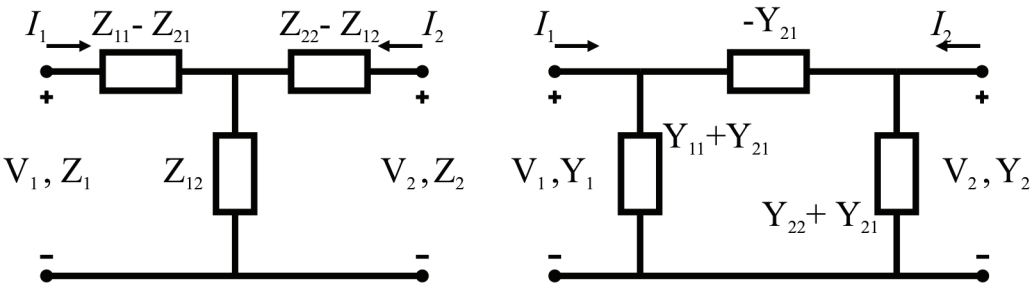

Figure 4. Coupling network models: (left) tee-network, (right) pi-network.

The similar procedure that we followed to build an equivalent network for a single meander coil will be applied here. Extra optimization goals will be added especially for the mutual impedance where the initial conditions for it have been obtained from the impedance matrix. A quarter wavelength transmission line that has been used in the equivalent circuit model of the single meander coil will be deleted in the equivalent circuit of two coupled coils to prevent any impedance transformation in the coupled impedance; an accurate equivalent circuit can thereby be generated, as shown in Figure 5. This circuit can be split up into three major parts: two series resonance circuits connected by a common tee-network representing the mutual coupling between two elements. After several iterative simulations based on a random method offered by the ADS simulator, the

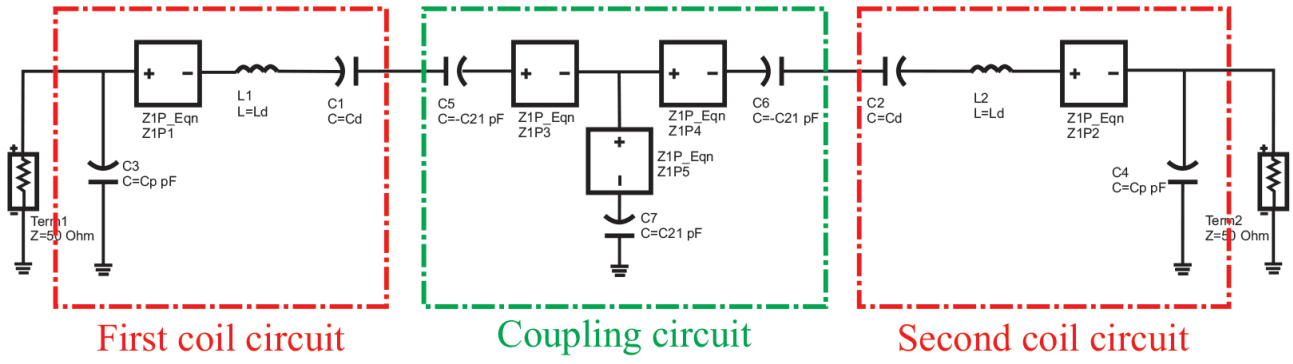

Figure 5. Equivalent circuit of two-parallel meander coils.

mutual impedance had a value of 3.3-j*2.31 ohm. This value is very close to the value in the impedance matrix obtained by EM simulation.

Good agreement between results for meander coil input impedance and mutual impedance from EM and circuit simulations has been achieved, as shown in Figures 6a and 6b, respectively. From these results, we got the impression that the tee-network is a proper representative network for the parallel coupled meander coil.

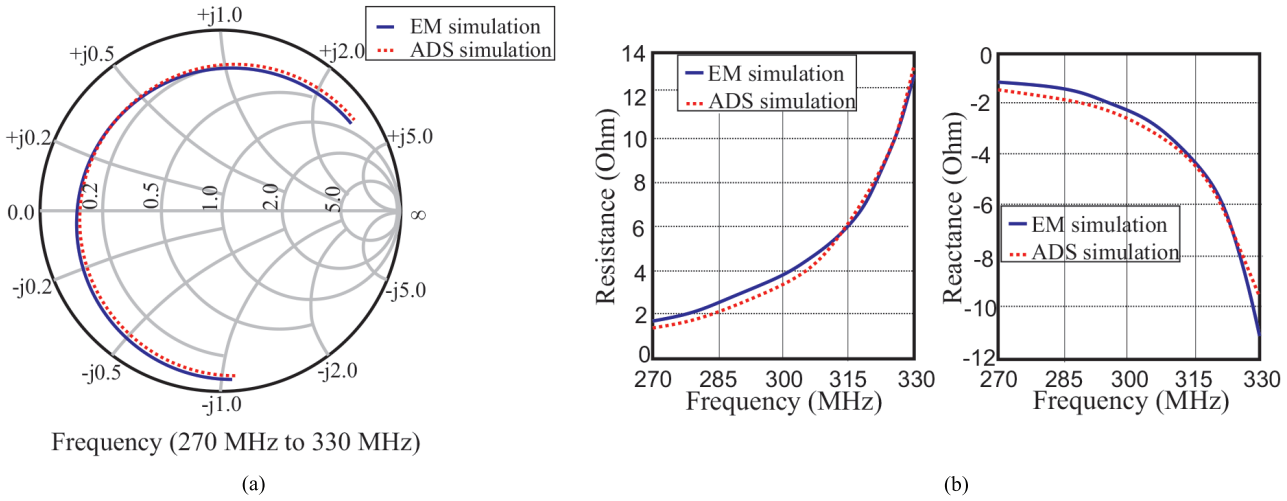

Figure 6. Impedance parameters of parallel meander coils: (a) input impedance of meander coil in Smith chart representation; (b) mutual impedance between two parallel meander coils: (left) resistance, (right) reactance.

2.2.2. Collinear meander coils

In Figure 7, two-coupled meander coils are collinearly aligned in free space below a homogeneous phantom. Similar to what we have done for parallel aligned coils, the S and Z parameter matrices have been obtained from the full-wave simulation as follows:

$$S = \begin{bmatrix} -0.6097 + j * 0.0003 & 0.3275 + j * 0.2823 \\ 0.3275 + j * 0.2823 & -0.6097 + j * 0.0003 \end{bmatrix}, \tag{5}$$

$$Z = \begin{bmatrix} 12.4638 + j * 4.5165 & 11.9134 + j * 11.8758 \\ 11.9134 + j * 11.8758 & 12.4638 + j * 4.5165 \end{bmatrix}. \tag{6}$$

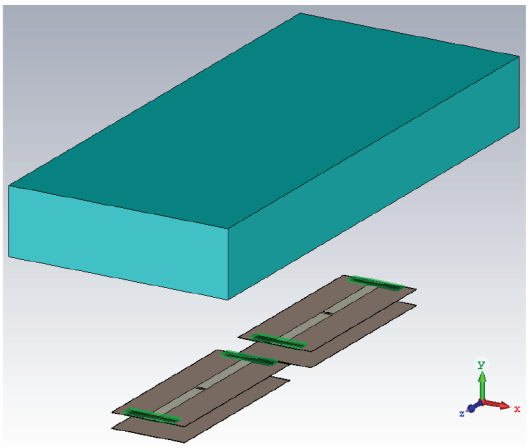

Figure 7. Simulation setup for two collinear meander coils in free space with a gap of 50 mm, situated 200 mm below a homogeneous phantom.

From the impedance matrix, the mutual reactance between both elements is inductive. A tee-network is used to model the equivalent circuit of two collinear meander coils. The mutual impedance obtained from the impedance matrix has been used as the initial condition in the circuit simulation. After several iterative simulations in the ADS simulator, an accurate equivalent circuit can be generated as shown in Figure 8, where the mutual impedance has a value of 11.55+j*12 ohm. This value again is very close to the value in the impedance matrix of EM simulation with good agreement between the results of meander coil input impedance and mutual impedance from EM and circuit simulations as shown in Figures 9a and 9b, respectively

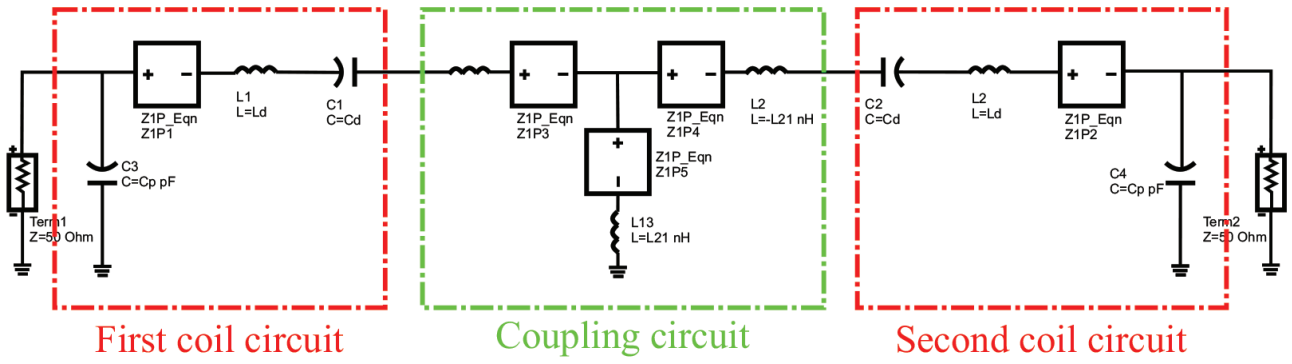

Figure 8. Equivalent circuit of two collinear meander coils.

2.3. Reactive element-based decoupling network

In [32], a decoupling network was proposed for wireless communications to isolate between two strongly coupled antennas. It consists of two transmission lines with characteristic impedance Z_o and electrical length θ, and a shunt reactive component with admittance jB as shown in Figure 10. The admittance Y_{21} appearing after the transmission lines would be purely imaginary and can thus be canceled by reactive component jB.
In [33], a similar decoupling network concept was used, replacing the transmission lines with reactive component jX instead. The closed-form equations for the elements of the decoupling network were given in the same paper.

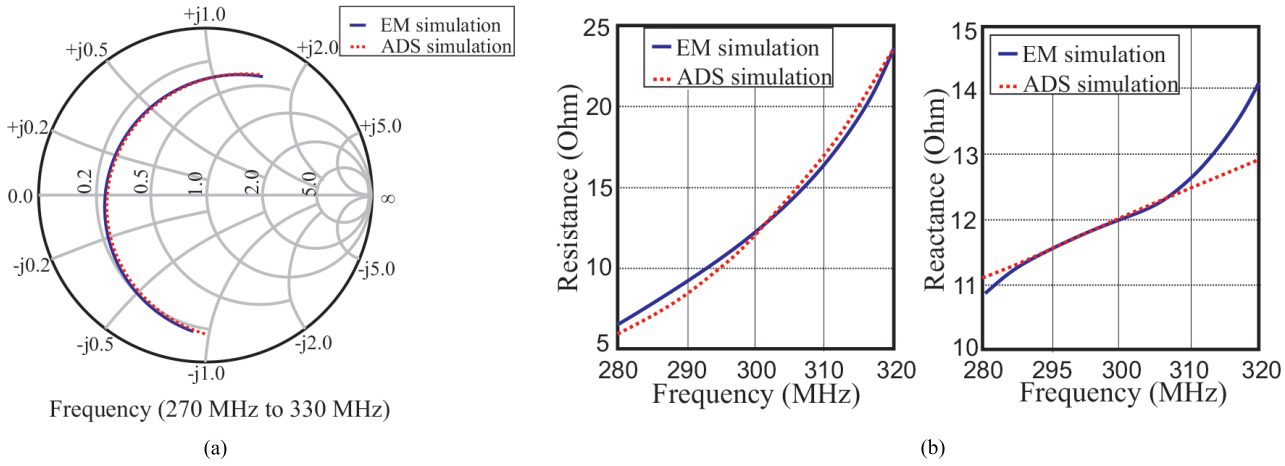

Figure 9. Impedance parameters of collinear meander coils: (a) input impedance of meander coil in Smith chart representation; (b) mutual impedance between two collinear meander coils (left) resistance, (right) reactance.

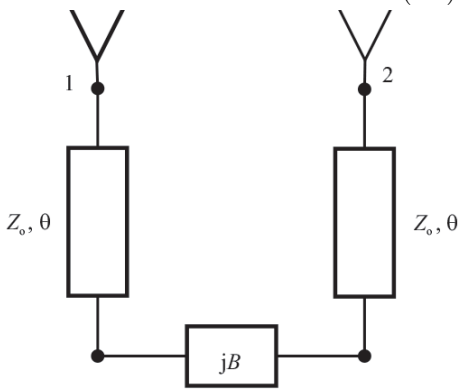

Figure 10. Reactive element-based decoupling network for two-coupled antennas.

3. Materials and methods

3.1. Decoupling networks for two-coupled coils

In this paper, the proposed decoupling networks for both coupled meander arrangements have made use of the design given in [33]. The values of the reactive components for both networks have been calculated based on the equations given in the same reference. For side-by-side arrangement, X = –7.5321 and B = –0.0528, and for collinear arrangement, X = 12.5765 and B = 0.0847. Now the decoupling networks are ready to be built up as shown in Figures 11a and 11b. Two series capacitors and one shunt inductor are needed for the first arrangement, whereas two series inductors and one shunt capacitor are needed for the second arrangement.

3.2. Decoupling network for coil arrays

Due to the promising results (e.g., image quality) achieved by using meander coils in 7T scanners, as mentioned before in this paper, several implementations have been done to build a Tx/Rx body coil using 8 channels [34, 35] or 32 channels [36, 37]. The 8-channel array in [34, 35] consists of 8 meander coils in a circular arrangement. In this case, the decoupling network in Figure 11 can be utilized to reduce the mutual coupling.

The body coil with 32 channels in [36, 37] is shown in Figure 12a. It consists of 32 meander coils arranged in 3 interleaved rings. One inner ring consists of 12 elements, while the two outer rings consist of 10 elements

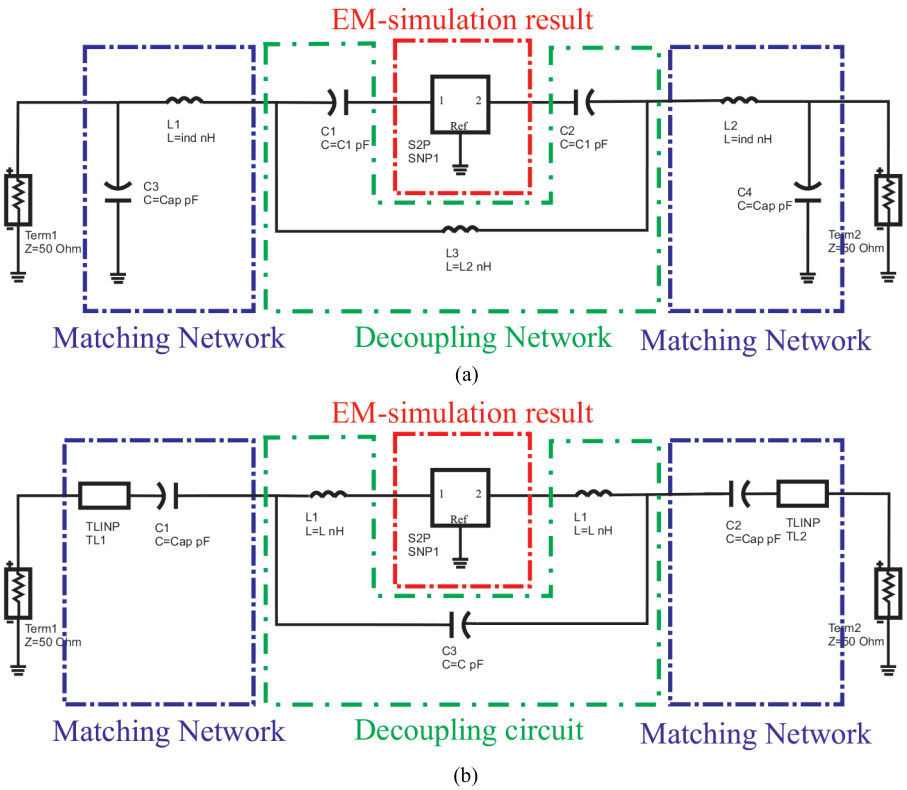

Figure 11. Decoupling networks for two different geometrical setups: (a) decoupling network for two parallel meander coils, (b) decoupling network for two collinear meander coils.

each. This body coil can be divided into eight subarrays with four meander coils each as shown in Figure 12b. The arrangement of coils 1 and 2 is considered collinear, whereas the arrangement of coils 3 and 4 is considered parallel. The decoupling networks for these two arrangements are discussed in Section 4.1. For the collinear arrangement, two inductors (L12) and one capacitor (C12) form the decoupling network, whereas one inductor (L34) and two capacitors (C34) form the decoupling network for the parallel arrangement as shown in Figure 13. The T-shaped decoupling networks in the same figure are used to decouple coils 1&2 from coils 3&4. They consist of two inductors (L21), two resistors (R1), and one shunt capacitor (C1). This decoupling network was proposed in [38] for MIMO applications. It has been used to decouple between two strongly coupled antennas and to provide wideband isolation.

4. Results

Both decoupling networks illustrated in Figures 11a and 11b show high isolation between the coupled meander coils. For parallel arrangement, isolation of more than 60 dB has been obtained between the coupled meander coils after adding the corresponding decoupling network, whereas the isolation was around 10 dB without the decoupling network as seen in Figures 14a and 14b.

For collinear arrangement, isolation of more than 60 dB has been obtained between the coupled meander coils after adding the corresponding decoupling network, whereas the isolation was around 5 dB without the decoupling network as seen in Figures 14c and 14d.

In the case of a 32-channel body coil, three different decoupling networks have been proposed as shown in Figure 13. After optimizing the values of the decoupling networks elements, isolation of more than 40 dB

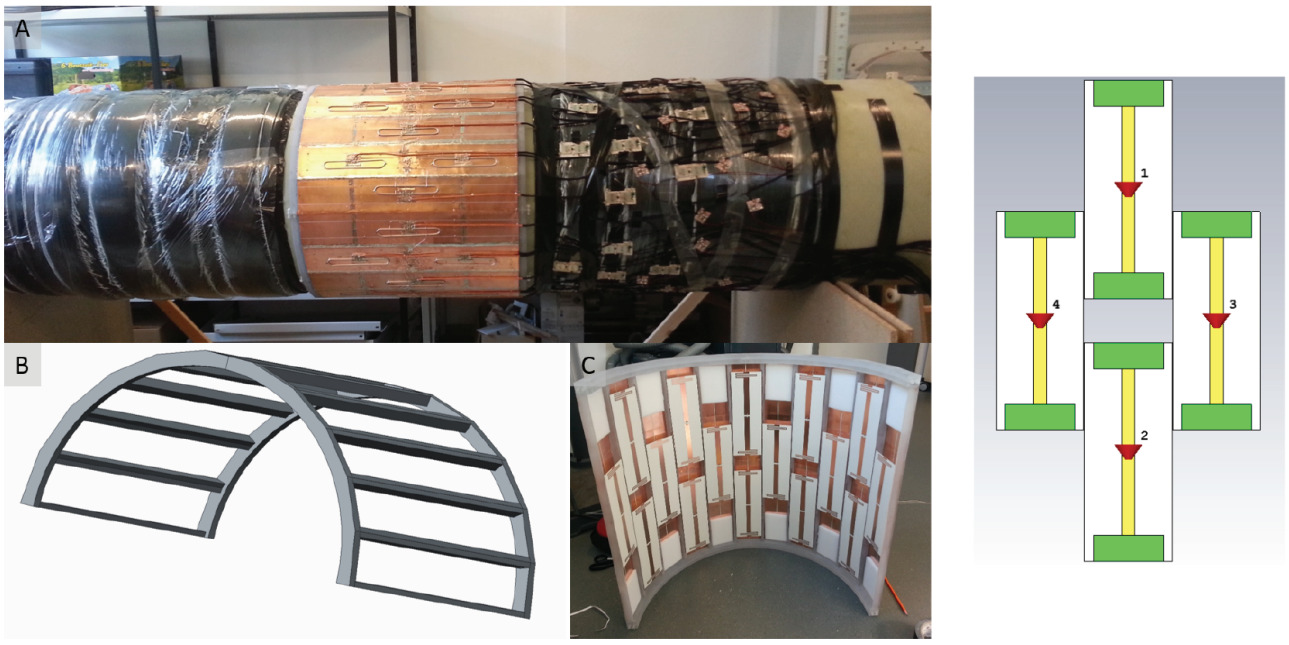

(a) (b)

Figure 12. A body coil for 7T whole body imaging: (a) a 32-channel body coil for 7 T [36], (b) simulation setup for four meander coils, representing one subarray in the 32-channel body coil.

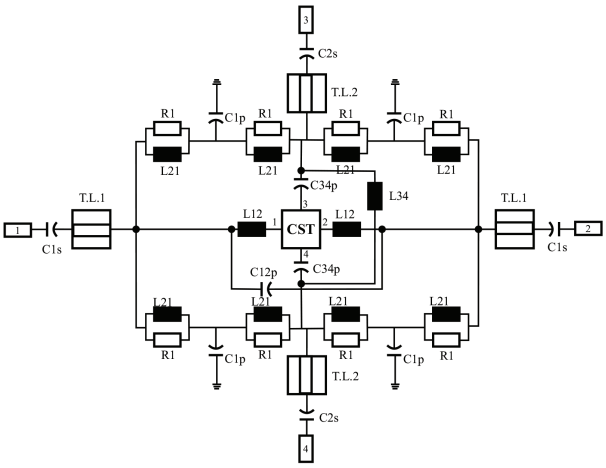

Figure 13. Decoupling network for one subarray in the 32-channel body coil.

has been obtained between the four meander coils in the subarray as shown in Figure 15a, whereas the mutual coupling between the subarray elements before adding the decoupling networks is shown in Figure 15b. Table 1 summarizes the values of all decoupling networks elements. The matching network for all meander coils consists of a transmission line connected in series with capacitor. For coils 1&2, the transmission line (T.L. 1) with series capacitor (C1s) form the matching network, whereas the transmission line (T.L. 2) with series capacitor (C2s) form the matching network for coils 3&4. Table 2 summarizes the values of all matching networks elements.

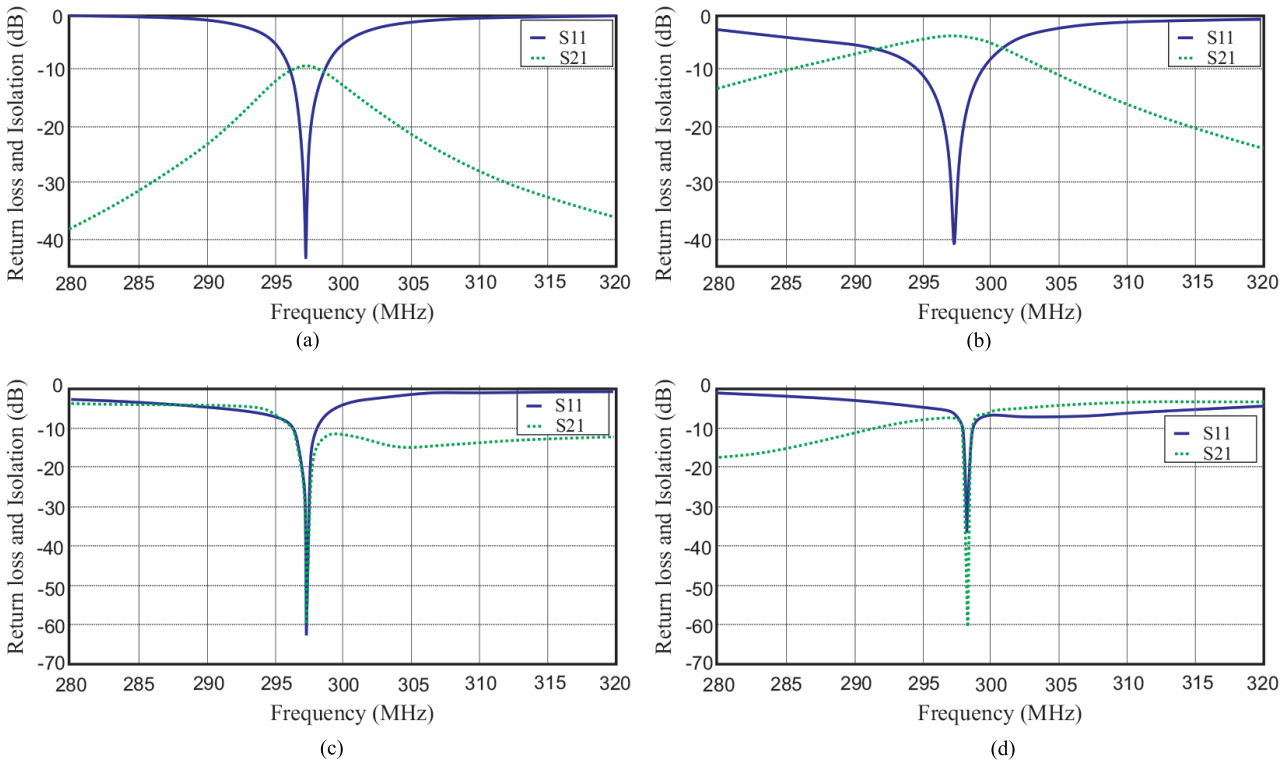

Figure 14. S-parameters for two-coupled meander coils with and without decoupling network: (a) return loss and isolation before adding decoupling network and with matching network for parallel meander coils, (b) return loss and isolation after adding decoupling network and matching network for parallel meander coils, (c) return loss and isolation before adding decoupling network and with matching network for collinear meander coils, (d) return loss and isolation after adding decoupling network and matching network for collinear meander coils.

Table 1: The values of all decoupling networks elements, which are shown in Figure 13.

Network	Decoupling network 1		Decoupling network 2		Decoupling network 3		
Component	L12 (nH)	C12 (pF)	L34 (nH)	C34 (pF)	L21 (nH)	C1 (pF)	R1 (ohm)
Value	12.3	25	150	12	30	85	50

Table 2: The values of all matching networks elements, which are shown in Figure 13.

Network	Matching network 1		Matching network 2	
Component	C1s (pF)	T.L.1	C2s (pF)	T.L.2
Value	4.8	Epsilon=2.3 length= 116 mm Zo=50 ohm Attenuation=0.478	10	Epsilon=2.3 length= 99 mm Zo=50 ohm Attenuation=0.478

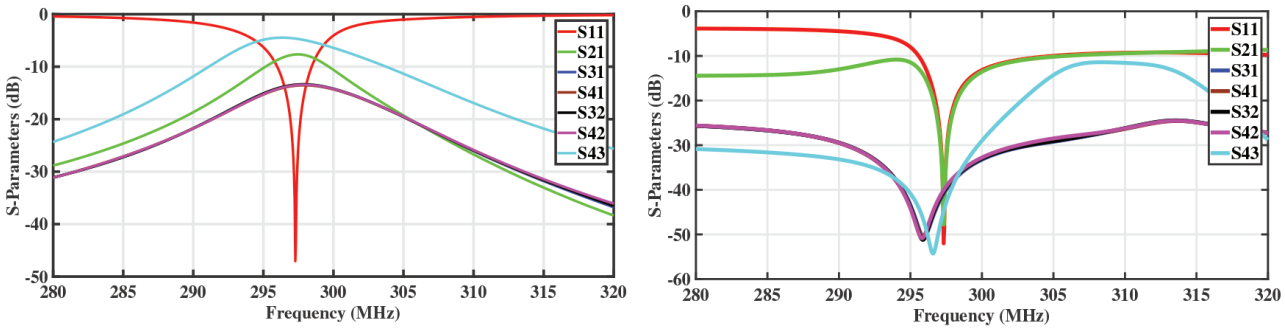

Figure 15. S parameters for one subarray in the 32-channel body coil: (a) S parameters with decoupling network, (b) S parameters without decoupling network.

5. Conclusion

This paper has studied the mutual coupling effect between two meander coils arranged in two different geometrical setups: parallel arrangement and collinear arrangement. Two different reactive component-based decoupling networks have been used to address the mutual coupling for both geometrical setups. Isolation enhancement for more than 50 dB has been obtained between the meander coils by using these decoupling networks in both arrangements. The recent proposed 32-channel body coil for 7 T is considered a more complex design that combines both previous arrangements in one design. The decoupling networks for such a complex coil have been designed and simulated in ADS. It has made use of the two previously discussed decoupling networks in addition to an extra decoupling network (T-shaped) to reduce the mutual coupling between adjacent array coil elements. The isolation performance has been investigated by designing four meander coils representing one subarray in the 32-channel body coil and integrating the three decoupling networks. High port isolation (more than 40 dB) has been achieved between array elements. A return loss of more than –40 dB has been obtained for all meander coils by adding matching networks composed of one 50 Ω transmission line with a specific length connected in series with the capacitor. The integrated decoupling networks in the subarray can be expanded to cover the rest of the subarrays in the 32-channel body coil. Hence, concurrent excitation for the multichannel RF body coil array can be accomplished.

Acknowledgment

This work was done at the Department of Electrical Engineering, Faculty of Engineering, Applied Science Private University, Amman, Jordan. The authors would like to thank the university for its strong support of this work.

References

[1] Yacoub E, Shmuel A, Pfeuffer J, Van De Moortele PF, Adriany G et al. Imaging brain function in humans at 7 Tesla. Magnetic Resonance in Medicine 2001; 45 (4): 588-594.

[2] Vaughan JT, Garwood C, Collins W, Liu L, DelaBarre G et al. 7T vs. 4T: RF power, homogeneity, and signal-to-noise comparison in head images. Magnetic Resonance in Medicine 2001; 46 (1): 24-30.

[3] Collins CM, Smith MB. Signal-to-noise ratio and absorbed power as functions of main magnetic field strength, and definition of 90° RF pulse for the head in the birdcage coil. Magnetic Resonance in Medicine 2001; 45 (4): 684-691.

[4] Hoult DI. Sensitivity and power deposition in a high-field imaging experiment. Journal of Magnetic Resonance Imaging 2000; 12 (1): 46-67.

[5] Van de Moortele PF, Akgun C, Adriany G, Moeller S, Ritter J et al. B1 destructive interferences and spatial phase patterns at 7 T with a head transceiver array coil. Magnetic Resonance in Medicine 2005; 54 (6): 1503-1518.

[6] Collins CM, Liu W, Swift BJ, Smith MB. Combination of optimized transmit arrays and some receive array reconstruction methods can yield homogeneous images at very high frequencies. Magnetic Resonance in Medicine 2005; 56 (6): 1327-1332.

[7] Mao W, Smith MB, Collins CM. Exploring the limits of RF shimming for high-field MRI of the human head. Magnetic Resonance in Medicine 2006; 56 (4): 918-922.

[8] Katscher U, Börnert P, Leussler C. Transmit SENSE. Magnetic Resonance in Medicine 2003; 49 (1): 144-150.

[9] Grissom W, Yip CY, Stenger VA, Fessler JA, Noll DC. Spatial domain method for the design of RF pulses in multicoil parallel excitation. Magnetic Resonance in Medicine 2006; 56 (3): 620-629.

[10] Orzada S, Maderwald S, Poser B, Bitz AK, Quick HH et al. RF excitation using Time Interleaved Acquisition of Modes (TIAMO) to address B1 inhomogeneity in high-field MRI. Magnetic Resonance in Medicine 2010; 64 (2): 327-333.

[11] Aussenhofer S, Webb AA. An eight-channel transmit/receive array of TE01 mode high permittivity ceramic resonators for human imaging at 7T. Journal of Magnetic Resonance 2014; 243: 122-129.

[12] Kraff O, Bitz A, Kruszona S, Orzada S, Schaefer L et al. An eight-channel phased array RF coil for spine MR imaging at 7 T. Investigative Radiology 2009; 44 (11): 734-740.

[13] Salama S. Design of a rectangular loop-shape RF coil for 7-Tesla Magnetic Resonance Imaging. In: IEEE Asia Pacific Microwave Conference; Kuala Lumpur, Malaysia; 2017. pp. 1044-1047.

[14] Zhang X, Ugurbil K, Kruszona S, Chen W. Microstrip RF surface coil design for extremely high-field MRI and spectroscopy. Magnetic Resonance in Medicine 2001; 46: 443-450.

[15] Raaijmakers AJ, Ipek O, Klomp DW, Possanzini C, Harvey P et al. Design of a radiative surface coil array element at 7 T: the single-side adapted dipole antenna. Magnetic Resonance in Medicine 2011; 66: 1488-1497.

[16] Hong SM, Park JH, Woo MK, Kim YB, Cho ZH. New design concept of monopole antenna array for UHF 7T MRI. Magnetic Resonance in Medicine 2014; 71 (5): 1944-1952.

[17] Roemer PB, Edelstein WA, Hayes CE, Souza SP, Mueller OM et al. The NMR phased array. Magnetic Resonance in Medicine 1990; 16 (2): 192-225.

[18] Lee RF, Giaquinto RO, Hardy CJ. Coupling and decoupling theory and its application to the MRI phased array. Magnetic Resonance in Medicine 2002; 48 (1): 203-213.

[19] Mahmood Z, Guérin B, Adalsteinsson E, Wald LL, Daniel L. An automated framework to decouple pTx arrays with many channels. In: Proceedings of 21st Annual Meeting of ISMRM; Salt Lake City, UT, USA; 2013. p. 2722.

[20] Jevtic J. Ladder networks for capacitive decoupling in phased-array coils. In: Proceedings of the 9th Annual Meeting of ISMRM; Glasgow, UK; 2001. pp. 17.

[21] Wu B, Zhang X, Qu P, Shen GX. Design of an inductively decoupled microstrip array at 9.4 T. Journal of Magnetic Resonance 2006; 182 (1): 126-132.

[22] Salama S. Reactive-element based decoupling network for a two-element MRI phased array. Journal of King Saud University-Engineering Sciences (in press). doi: 10.1016/j.jksues.2018.05.003

[23] Abuelhaija A, Orzada S, Solbach K. Parasitic element based decoupling of 7 Tesla MRI coil array. In: Loughborough Antennas & Propagation Conference; Loughborough, UK; 2015. pp. 1-5.

[24] Yan X, Zhang X, Wei L, Xue R. Magnetic wall decoupling method for monopole coil array in ultrahigh field MRI: a feasibility test. Quantitative imaging in Medicine and Surgery 2014; 4 (2): 79.

[25] Salama S, Abuelhaija A. Parasitic element based decoupling network for a two-element MRI Phased Array. In: IEEE Jordan International Joint Conference on Electrical Engineering and Information Technology; Amman, Jordan; 2019. pp. 790-793.

[26] Abuelhaija A, Solbach S. An ultra-low output impedance power amplifier for Tx Array in 7-Tesla magnetic resonance imaging. Journal of Magnetic Resonance 2015; 2 (8): 1422.

[27] Abuelhaija A, Solbach S, Buck A. Power amplifier for magnetic resonance imaging using unconventional Cartesian feedback loop. In: German Microwave Conference; Nürnberg, Germany; 2015; pp. 119-122.

[28] Brunner DO, De Zanche N, Froehlich J, Baumann D, Pruessmann K. A symmetrically fed microstrip coil array for 7T. In: 15th Proceedings of International Society of Magnetic Resonance in Medicine; Berlin, Germany; 2007. p. 448.

[29] Orzada S, Bahr A, Bolz T. A novel 7 T microstrip element using meanders to enhance decoupling. In: 16th Proceeding of International Society for Magnetic Resonance in Medicine; Toronto, Canada; 2008. p. 2979.

[30] Gmeel S, Solbach K, Rennings A, Chen Z. SAR reduction for dipole RF coil element at 7 Tesla by using dielectric overlay. In: Loughborough Antennas & Propagation Conference (LAPC); Loughborough, UK; 2012. pp. 1-3.

[31] Abuelhaija A, Solbach S, Orzada S. Comprehensive study on coupled meandered microstrip line RF coil elements for 7-Tesla magnetic resonance imaging. In: 9th European Conference on Antennas and Propagation; Lisbon, Portugal; 2015. pp. 1-5.

[32] Chen SC, Wang YS, Chung SJ. A decoupling technique for increasing the port isolation between two strongly coupled antennas. IEEE Transactions on Antennas and Propagation 2008; 56 (12): 3650-3658.

[33] Coetzee J, Yu Y. Closed-form design equations for decoupling networks of small arrays. Electronics Letters 2008; 44 (25): 1441-1442.

[34] Orzada S, Bitz A, Johst S, Gratz M, Völker MN et al. An integrated 8-channel Tx/Rx body coil for 7 Tesla whole-body MRI. Frontiers in Physics 2017; 5: 17.

[35] Orzada S, Bitz A, Gratz M, Johst S, Völker MN et al. An integrated 8-channel Tx/Rx body coil for 7 Tesla whole-body MRI. In: Proceedings of the 23th Annual Meeting of ISMRM; Toronto, Canada; 2015. p. 630.

[36] Orzada S, Bitz A, Gratz M, Johst S, Shooshtary S et al. A 32-channel transmit system add-on for 7 Tesla body imaging. In: Proceedings of the 25th Annual Meeting of ISMRM; Honolulu, HI, USA; 2017. p. 1219.

[37] Orzada S, Bitz A, Kraff O, Gratz M, Oehmigen M et al. A 32-channel integrated body coil for 7 Tesla whole-body imaging. In: Proceedings of the 24th Annual Meeting of ISMRM; Singapore; 2016. p. 167.

[38] Li L, Venkatasubramanian S, Lehtovuori A, Icheln C, Heino M et al. T-shaped decoupling network for wideband isolation improvement between two strongly coupled antennas. In: Loughborough Antennas & Propagation Conference (LAPC); Loughborough, UK; 2015. pp. 1-4.